Surface roughness of pyroclastic deposits at Mt. Etna by 3D laser scanning

Francesco Mazzarini ([1]), **Massimiliano Favalli** ([1]), **Ilaria Isola** ([1]), **Marco Neri** ([2]) **and Maria Teresa Pareschi** ([1])
([1]) *Istituto Nazionale di Geofisica e Vulcanologia, Sezione Pisa, Italy*
([2]) *Istituto Nazionale di Geofisica e Vulcanologia, Sezione Catania, Italy*

Abstract
The terrestrial 3D Laser Scanning technique was applied to analyse the surface roughness of pyroclastic deposits on volcanic surfaces at Mt. Etna. This technique allowed the construction of high accuracy digital elevation models of small surfaces, about 1 m across. Sampled surfaces differ for percentage of coverage and for grain size of the pyroclastic deposits. The change in grain size distribution for the pyroclastic unconsolidated deposits affects the surface roughness. The roughness of the site where the finest pyroclastic deposits occur is mainly governed by large scale wavelength morphology (Hurst exponent H = 0.77 for lengths larger than 16 mm). The other sampled surfaces have self-affine characters with low (0.15) to intermediate (0.35 - 0.38) Hurst exponents for lengths higher than 10-22 mm. Here we show results of the analysis of the surface roughness of the pyroclastic deposits emplaced during the 2001 and 2002-2003 eruptions at Mt. Etna. Grain size and thickness of pyroclastic deposits mainly control the overall roughness of such as volcanic surface.

Key words *surface roughness – pyroclastic deposits – Laser 3D – Mt. Etna*

1. Introduction

The roughness of natural surfaces on the Earth and on terrestrial planets is defined as the topographic expression of a surface at horizontal scale from sub-metre to hundreds of metres (Shepard *et al*., 2001). It strongly affects the brightness, polarization and angular scattering properties of reflected and emitted energy in optical, infrared and microwave remote sensing applications (Campbell and Shepard, 1996; Akiyama and Sasaki, 2002; Butler *et al*., 1998). Topographic data for wide areas are derived from optical and radar sensors mounted in airplane or satellite platform in planetary geology and in volcanology (Orosei *et al*., 2003; Mazzarini *et al*. 2005; 2007; Morris *et al*., 2006). In the field of volcanology, the structure and roughness of lava flows provide information on flow emplacement parameters and on flow rheology (Bulmer *et al*., 2001; Morris *et al*., 2006; Pesci *et al*., 2007), or defining ground deformation patterns in lava fields by using InSAR data (Briole *et al*., 1997; Amelung *et al*., 2000; Froger *et al*., 2001; Stevens *et al*., 2001). Topographic data of volcanic surfaces are gathered from laser profilers, line and transit, stereo-photography, differential GPS methodologies (Shepard *et al*., 2001), as well as through very high resolution multibeam technique in marine and crater lake volcanoes (Anzidei *et al*., 2006; Anzidei *et al*., 2008; Morgan *et al*., 2003).

The smooth or rough appearance of a surface is a function of the incident energy wavelength (λ). Following the Rayleigh Criterion, a surface is smooth if $h < \lambda/8\cos\theta$, where h is the standard deviation of surface relief and θ is the incident angle; surface roughness is crucial for microwave applications since the used wavelengths may vary between 1 to 100 cm

Mailing address: Dr. Francesco Mazzarini, Istituto Nazionale di Geofisica e Vulcanologia, Via della Faggiola, 32, 56126 Pisa, Italy; email: mazzarini@pi.ingv.it

(Janza *et al*., 1975; Shepard *et al*., 2001). Natural volcanic surfaces like pāhoehoe basaltic lava flows have an average roughness value of 11.04 +/- 5.47 cm (Campbell and Shepard, 1996; Shepard *et al*., 2001), and the roughness of ‘a‘ā flows (spiny and blocky surfaces) is expected to be higher than that of pāhoehoe flows (a few centimetres to several tens of centimetres). Smoother surfaces are expected for pyroclastic products that often drape the flanks of large volcanoes. In unconsolidated deposits (such as pryroclastic deposits) at the scale of observation of millimeters or meters the change in grain size may result in a significant change in the surface texture and surface roughness.

In order to analyze and define the surface roughness of the volcanic rocks at Mt. Etna, a field survey was done in September 2005 to acquire topographic information on surfaces 0.5 - 1 m wide. The surface topography was acquired by using a portable terrestrial 3D Laser Scanner, producing detailed digital elevation models of volcanic surfaces up 0.7 m wide with vertical resolution less than 0.5 mm. This contribution focuses on pyroclastic deposits (scoriae, lapilli and ash) erupted in the last few years (2000-2003) that mantled the eastern and southern flanks of the volcano (Andronico *et al*., 2005; Casacchia *et al*., 2006; Sgavetti *et al*., 2006). In the following we refer to these pyroclastic deposits as tephra.

The presented analysis of high-resolution digital elevation models of tephra on active volcanoes could thus represent a powerful tool to identify pyroclastic cover in active volcanoes; this approach could be especially useful in remote and inaccessible volcanic areas.

2. Mt. Etna test sites

Mt. Etna (fig. 1), located on the east coast of the island of Sicily (Italy), with a basal diameter of about 40 km, is the highest volcano in Europe. Its activity is characterised by effusive and some explosive summit and flank eruptions (Branca and Del Carlo, 2004; Behncke *et al*., 2005). Recently, during the 2001 and 2002-2003 eruptions, new vents formed on its southern flank as well as new fractures along the north-eastern slope, with the production of significant volumes of tephra (Taddeucci *et al*., 2002; Behncke and Neri, 2003a; 2003b; Andronico *et al*., 2005; Allard *et al*., 2006). The latter are composed by non-vesicular to highly vesicular glass, crystals (plagioclase, pyroxene and olivine), lithic clasts (altered volcanic and sedimentary rocks) and tachylite clast. The ash comprised tachylite, sideromelane, crystals and lithic clasts, the relative proportions of which changed throughout the eruption. Generally, lithic and crystal contents of 2002-2003 eruptions were lower than during the 2001 eruption (Taddeucci *et al*., 2002; Andronco *et al*., 2005). Copious tephra covered the flanks of the volcano, particularly on its eastern and south-eastern sectors, due to the prevailing wind direction that driven its deposition (Favalli *et al*., 2004). More information on the recent eruptive history along with a daily update of Mt. Etna activity, is available at the INGV website (www.ct.ingv.it).

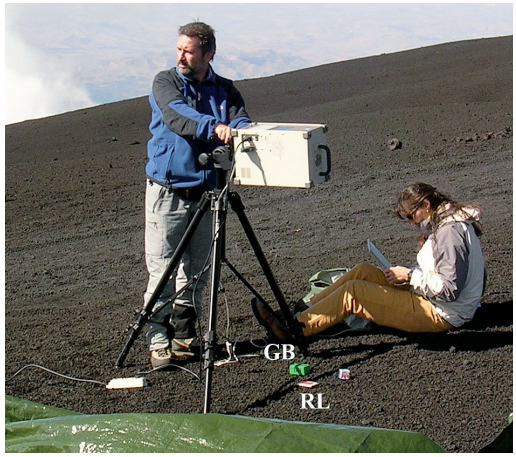

Fig. 1. The Konica Minolta VI-910 3D digitizer mounted on the tripod elevated about 1 m above the ground surface covered by coarse grained tephra, just north of the 2002-2003 vents (Sample S8 in fig. 2). Green box (GB) and red labels (RL) below the Laser 3D are used as reference features. The green canvas in the foreground is used to reduce the environment illumination.

3. Data acquisition

The local morphologies of volcanic surfaces formed by tephra and by lava with variable amount of tephra coverage have been derived by a 3D scansion of the surface by a terrestrial Laser scanner device. We used a Konica Minolta VI-910, which is a remote non-contact 3D digitizer (www.konicaminolta-3d.com), to derive through Laser triangulation x, y and z coordinates of imaged objects. The objects are scanned by a plane of laser light launched from the VI-910's source aperture. The Laser light (690 nm) is reflected from the surface of the scanned object and registered by the instrument. Each scan line is observed by a single frame and captured by a CCD camera. The surface shape is converted to a grid of over 300,000 vertices (connected points). The VI-910 is provided with three interchangeable lenses that can accommodate measurement of objects of various sizes and distances from the lens. A single scan is capable of capturing an angular field of view of approximately 10 cm^2 (TELE lens) to 0.8 m^2 (WIDE lens). The scansion has an accuracy of 0.22 mm in x, 0.16 mm in y and 0.1 mm in z axis for the TELE lens with 300,000 vertices. The WIDE lens accuracy is 1.4 mm along x, 1.04 mm along y and 0.4 mm along z; the z axis is the optical axis of the laser scanner. During measurements, the laser is mounted on a tripod and positioned at nadir with respect to the surface (fig. 1). In such a way, the z values are the elevation of the surfaces. The surfaces sampled at Mt. Etna have areas in the range of 0.17 – 0.24 m^2 imaged at a distance of about 90- 100 cm.

The topography of surfaces mantled by tephra was sampled in four sites (fig. 2). Sample 8 (S8) is located at about 0.4 km north of the 2002-2003 eruptive vents at an elevation of 2930 m. Grain size of such a proximal tephra is in the range 4-2 mm with some scoria up to 16 mm (Casacchia *et al*., 2006). Samples 9 (S9) and 10 (S10) are 2 km north-west of the 2002-2003 vents at an elevation of 3016 m overemplaced the 1999 lava field (Calvari *et al*., 2002). The 48 % of the S9 and the 84 % of the S10 sampled surfaces are covered by tephra, respectively. Sample 11 (S11) is located at about 4 km south-south east of the 2002-2003 eruptive vents at an elevation of 1812 m (fig. 2). Grain size of such a distal tephra is in the range 0.25 - 0.10 mm (Casacchia *et al*., 2006). For each sampled site, the photo of the viewed area is acquired and from elevation data a shaded relief image is derived (fig. 3). All the measurements have been collected using the WIDE lens in use with the instrument.

4. Surface roughness

In order to qualitatively describe the surface roughness the Root Mean Square of Heights (σ), the Allan Deviation (ν), and the autocorrelation Length (λ) have been computed for each sample see (Shepard *et al*., 2001).

The Root Mean Square of Heights (σ) is defined as:

$$\sigma = \left\{ \frac{1}{n-1} \sum_{i=1}^{n} \left[z(x_i) = \bar{z} \right]^2 \right\}^{1/2} \qquad (4.1)$$

where $z(x_i)$ is the elevation of point in position x_i, $\bar{Z}$ the average elevation and n is the number of points. The σ was computed over the whole area, the surfaces were de-trended (Shepard *et al*., 2001) by subtracting the best-fit plane. The lower the σ, the smoother the surface.

The Allan Deviation or Root Mean Square deviation (ν) is a function of the Δx lag, and is defined as:

$$\nu\left(\Delta x = \left\{ \frac{1}{n} \sum_{i=1}^{n} \left[z(x_i) - z(x_i + \Delta x) \right]^2 \right\}^{1/2} \right) \qquad (4.2)$$

where $z(x_i)$ is the elevation of point of position x_i, n is the number of points, and Δx is the lag used. The function $\nu(\Delta x)$ is computed averaging both horizontal and vertical de-trended profiles derived from 3D Laser scansion.

The autocorrelation function was computed over horizontal and vertical de-trended profiles

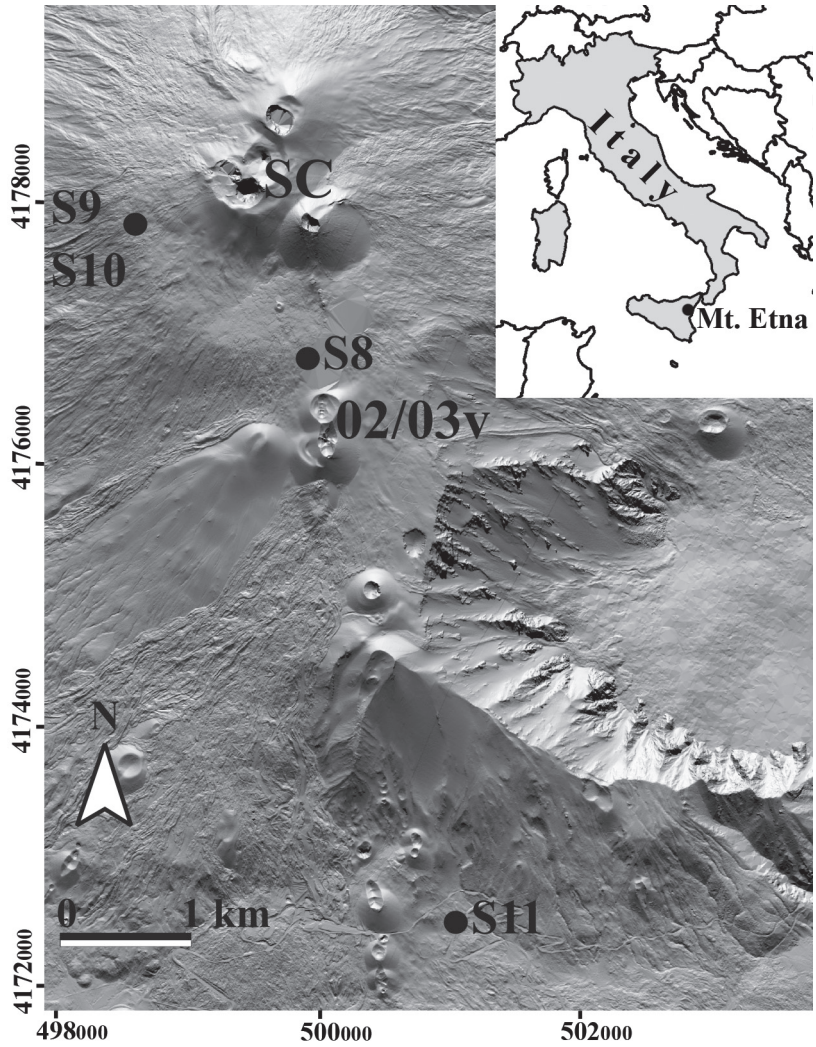

Fig. 2. Location of sampled sites at Mt. Etna. The shaded image is derived from September 2004 LiDAR elevation data (Mazzarini *et al*., 2007). SC: summit craters; 02/03v: vents formed during the 2002-2003 eruption (Andronico *et al*., 2005). Image is illuminated from north and georeferred in UTM projection, Zone 33 N, WGS 84 datum, labels in left and in bottom sides of figure are UTM coordinates (m).

as function of the Δx lag as described in (Shepard *et al*., 2001). The autocorrelation length (λ) is thus defined as the distance or lag for which the autocorrelation reduces to 1/e *i.e.* of ~37%.

Topography of natural surfaces is assumed to be self-affine such that increasing the scale of the x and y axes by a factor r must be compensated for in the z direction by a factor r^H, where H is the Hurst exponent ($0 < H < 1$). In the case $H = 0$, the $\nu(\Delta x)$ or $\sigma(\Delta x)$ are independent of the scale of observation (the profile length, for example). The case $H = 0.5$ is often observed in nature and often

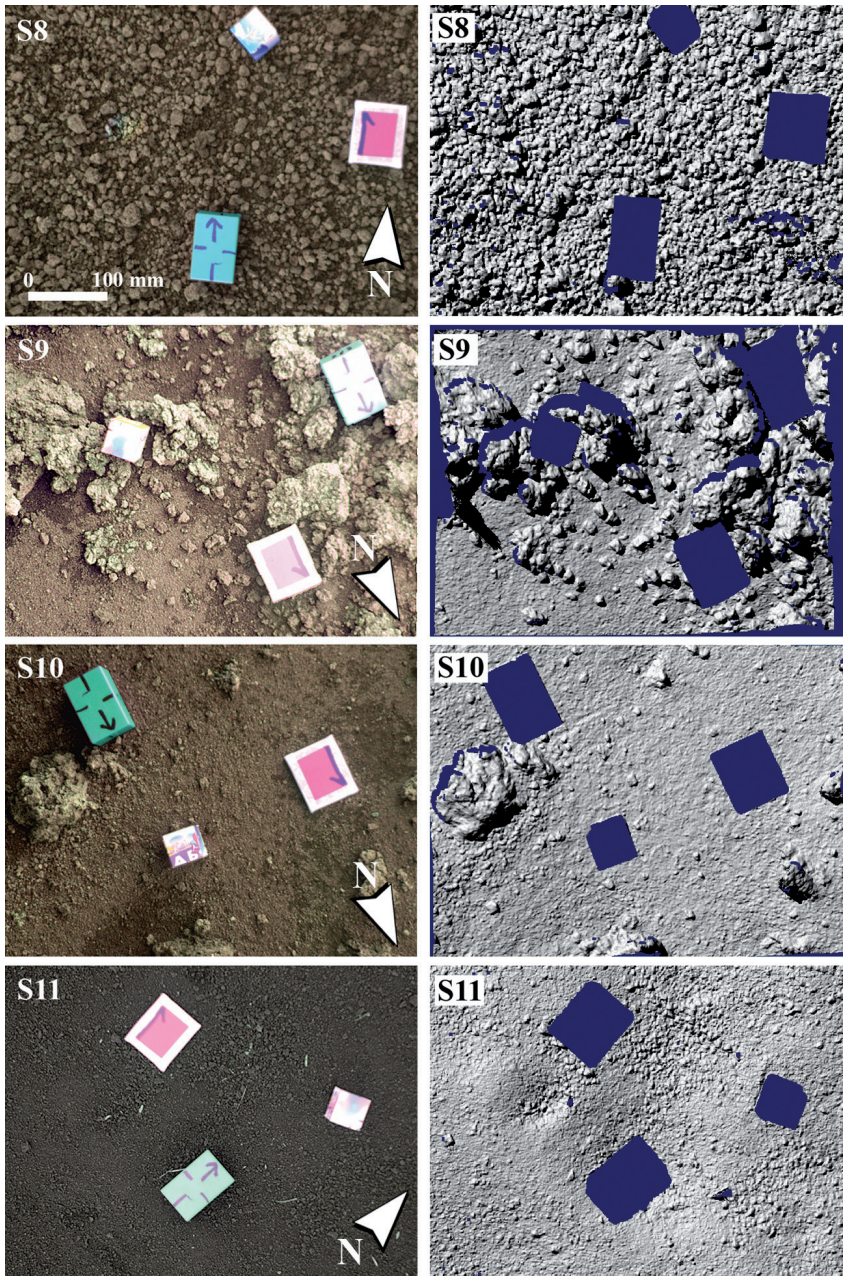

Fig. 3. Left column: RGB 24 bit colour images of the sampled surfaces acquired during 3D Laser scansion by a CCD camera. Right column: Shaded images (illumination from the top) of the digital elevation models of sampled surfaces. Scale bar shown on the top left corner image, is the same for all images. Coloured boxes and panels on figures (blue areas on shaded images) are reference features used to construct DEM of surfaces. The white arrows show North.

referred as Brownian noise (Turcotte, 1997). Finally, the $H = 1$ case, results in a self-similar behaviour of topography, that is z scales as x and y. Visually, the effect of this property is that surfaces with $H > 0.5$ look smoother than surfaces with $H < 0.5$ (Shepard *et al.*, 1995; Campbell and Shepard, 1996; Shepard and Campbell, 1999; Shepard *et al.*, 2001). The Hurst exponent is related to the commonly used fractal dimension D, by $D = 2 - H$ in the case of a profile and $D = 3 - H$, for a surface.

For an ideal fractal, the conventional parameters σ and ν, among other, change with scale, while H is strictly the same.

In order to derive H, we start by computing ν, as in (4.2), for different values of the step size Δx. If topography is indeed self-affine, equation (4.3) holds:

$$\nu(\Delta x) = C \times \Delta x^{H} \qquad (4.3)$$

where C is a constant.

Thus, H is derived as the slope of the best fit line of log $\nu(\Delta x)$ vs. log Δx. The computation of H is done in the length range where the curve exhibits a linear trend. In table I all the computed parameters in the four sampled sites are listed.

5. Discussion

The computed σ and λ well define the surface roughness as confirmed also by visual inspection (fig. 3). The S8 sample has σ (4.3 mm) and λ (9.8 mm) that well describe the surface mainly constituted by scoriae of about 5-10 mm in size (fig. 3; table I). Sample S9 (48% of tephra coverage) has the highest value of σ and an intermediate value of λ (table I). These values are well explained by the presence of large portions of lava (fig. 3). Sample S10 (84% of tephra coverage) has σ lower than that of S9 and λ similar to S9 (fig. 3 and table I). Finally, the S11 sample, whose surface is formed by small size objects (up to few mm; fig. 3), has the highest λ value and σ values much higher than the grain size (table I). The anomalous behaviour of the σ value in the S11 sample depends on the wavy pattern of the overall surface which masks the very small components due to the low grain size of the particles on the surface (fig. 4a).

According to equation (4.1), σ can be also computed for small portions (Δx^2) of the sampled surface. The curves $\sigma(\Delta x)$ *versus* Δx for the four samples are plotted in fig. 4b. In this way, it is possible to visualize the length range for which the large scale wavy patterns have low influence. At centimetre scale the S8 and

Table I. Roughness parameters of investigated sites.

Site	X (m)	Y (m)	Z (m)	A (m^2)	tfc %	σ (mm)	λ (mm)	H (R^2)	C	H range (mm)
S8	499943	4176781	2930	0.21	100	4.3	9.8	0.58 (*0.99*)	0.0763	1.8 – 6.3
								0.15 (*0.98*)	0.4562	9.9 – 63.9
S9	498625	4177813	3016	0.17	48	17.1	37.4	0.67 (*0.99*)	0.0966	1.2 – 16.8
								0.35 (*0.99*)	0.512	17.4 – 154.8
S10	498624	4177820	3016	0.20	84	7.8	37.4	0.66 (*0.99*)	0.2586	1.5 – 21.5
								0.38 (*0.99*)	0.1394	32 – 138.5
S11	501060	4172487	1812	0.24	100	8.6	64.4	0.47 (*0.99*)	0.2704	1.6 – 10.4
								0.77 (*0.99*)	0.5947	15.2 – 68
								0.63 (*0.99*)	0.3365	68.8 – 144

X: easting, Y: northing; Z: elevation (Projection UTM 33 – Datum WGS 84); A: sampled surface area; tfc: tephra coverage; σ: Root Mean Square of Heights; λ: autocorrelation Length; H: Hurst exponent; R^2: coefficient of correlation in the relative range (H range); C: normalization constant in equation 3.

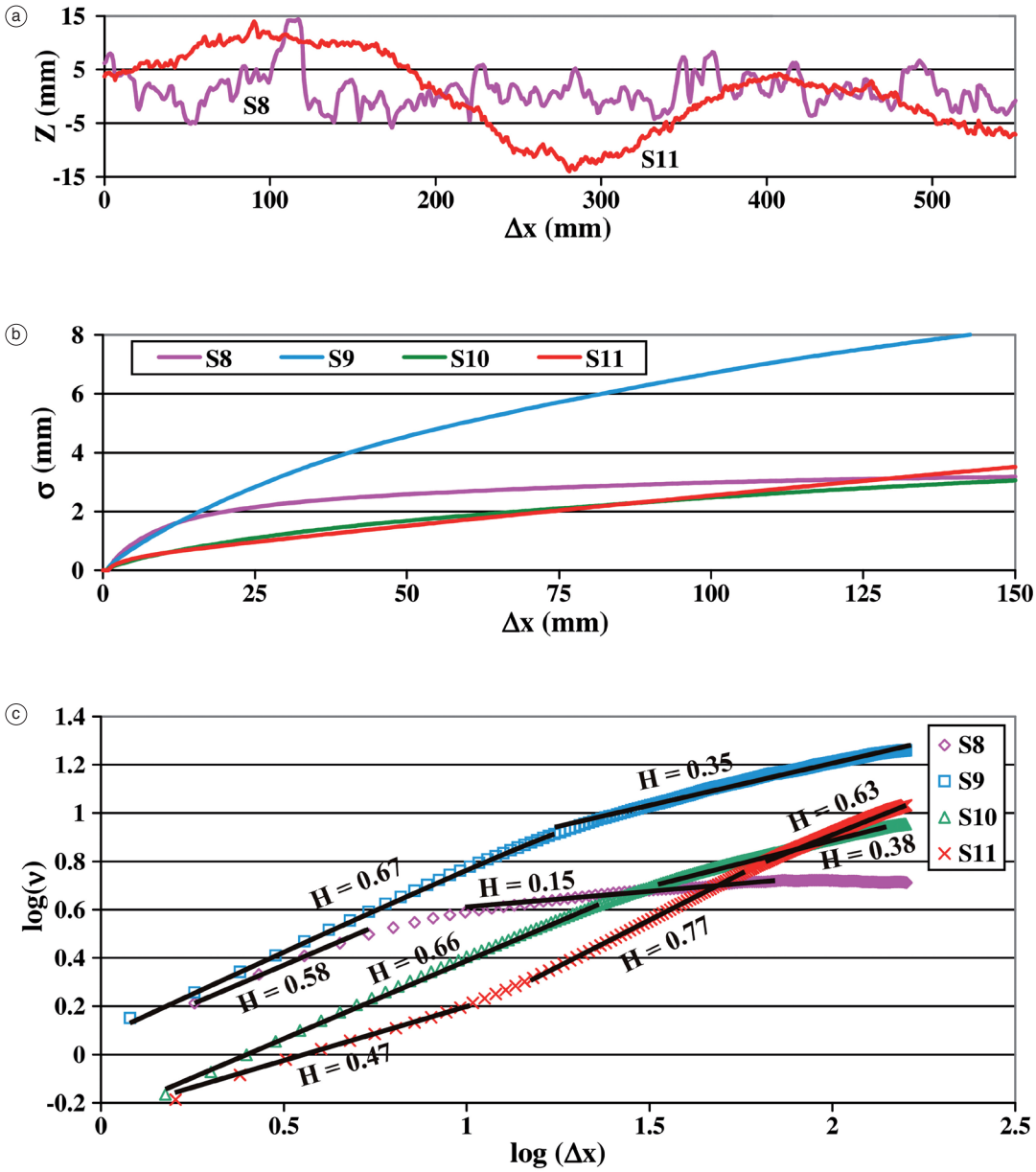

Fig. 4a-c. a) Plot of elevations (z) versus length (Δx) along de-trended horizontal profiles in the middle of the surfaces of samples S8 and S11. Note that large wavelength dominates in the distribution of heights in the S11 surface. b) Plot of σ (Δx) versus Δx for the sampled surfaces. At Δx lower than few centimetres, the surfaces S11 and S10 have lower σ values than S8 and S9 (see text for discussion). c) Log(v) vs log(Δx) plots for the sampled surfaces. The slope of the curves defines the Hurst exponent (H). In each curve, the best fit linear lines are outlined and the relative H values are reported. For each sample different H values exist at different scale range (see text).

Table II. Surface roughness of sampled tephra in the wavelength of Radar bands.

Radar band	λ range (cm)	λ (mm)	θ	ν(λ) (mm)	S8 H 0.58	S8 H 0.15	S9 H 0.67	S9 H 0.35	S10 H 0.66	S10 H 0.38	S11 H 0.47	S11 H 0.77	S11 H 0.63
Ka	0.8 -1.1	10	45	1.8	**4.5**	**4.0***	**5.8***	**7.3**	**2.5***	**3.3**	*1.6**	*1.5*	**2.0**
K	1.1 - 1.7	15	45	2.7	**5.7**	**4.3***	**7.7***	**8.4**	**3.3***	**3.9**	*1.9*	*2.1**	**2.5**
X	2.4 - 3.75	30	45	5.3	**8.6**	*4.8**	**12.2**	**10.7***	*5.2*	*5.0**	*2.7*	*3.5**	*3.9*
C	3.75 - 7.5	60	45	10.6	**12.8**	*5.3**	**19.4**	**13.6***	*8.2*	*6.5**	*3.7*	*6.0**	*6.1*
S	7.5 - 15	120	45	21.2	*19.2*	*5.9*	**31.0**	*17.4**	*13.0*	*8.5**	*5.1*	*10.2*	*9.4**
L	15 - 30	240	45	42.4	*28.6*	*6.5*	**49.1**	*22.1*	*20.5*	*11.1*	*7.1*	*17.3*	*14.6*
P	30 - 100	700	45	123.7	*53.3*	*7.6*	*100.7*	*32.2*	*41.6*	*16.6*	*11.7*	*39.5*	*28.6*

ν(λ): Allan Deviation for wavelength λ, θ: grazing incidence angle;: values computed in the range of validity of the H exponent (see table I). Bold: the surface is rough (ν(λ)<λ/8sin(θ)). Italics: the surface is smooth.*

S9 samples have high σ values, whereas the S11 and the S10 samples clearly show low σ values (fig. 4b). This behaviour is due to the presence in the S8 and S9 surface of centimetre sized features (fig. 3). On the other hand, S11 and S10 surfaces are mostly formed by millimetre and sub-millimetre sized features (fig. 3).

The presence of small and large scale components in the surface roughness is well outlined by the computed H exponents. All the sampled surfaces depart from a strict power law representing the ideal model and show a complex behaviour: they roughen in different ways at different scales (table I). Samples S8, S9 and S10 have very similar behaviours; they have H in the range 0.58 – 0.67 mm at small scale and have a transition to H in the range 0.15 – 0.38 mm at larger scales (fig. 4c and table I). At large scale, the S8 sample has very low H = 0.15 since the surface is dominated by small scale (~9 mm) grains (fig. 3); that is, the surface gets rapidly smooth as the scale increases. S9 and S10 have rather similar exponents at large scales (*i.e.* lengths greater than 22 mm) since their surfaces are formed by small tephra and larger lava blocks (fig. 3). Sample S11 has a quite different behaviour. S11 surface has H = 0.47 at small scale and above a threshold (~10 mm) it has very high H values (0.63 - 0.77). That is, the S11 surface, consisting of very fine grain-size tephra (fig. 3), tends to maintain its roughness as the scale increases.

Surface roughness has strong control over the backscatter signal in microwawe or Radar applications (*e.g.* Shepard *et al.*, 2001). Using the equation (4.2), the surface roughness of tephra at millimetre to centimetre scales (table I), and applying the Rayleigh Criterion (Janza *et al.*, 1975; Shepard *et al.*, 2001) we derive the roughness of sampled surfaces at the scale of radar bands (table II). Overall, tephra surfaces are smooth for wavelength larger than 6 cm (table II). Fine tephra (S11) look as smooth surface for all bands (table II); whereas, coarse tephra surface (S8) looks rough for small wavelength bands (bands Ka, K, table II). Moreover, as the fraction of tephra covering lava surfaces increases the surface gets smooth even for short wavelength (bands X and C, table II). As an example, InSAR applications use band C

(Amelung *et al*., 2000; Froger *et al*., 2001; Stevens *et al*., 2001), at the band C scale the lava flows covered by low fraction of tephra look rough.

6. Conclusions

The roughness of volcanic surfaces mainly formed by tephra were analysed at Mt. Etna. The 3D Laser Scanning method allows acquiring accurate morphologies of such as volcanic surfaces at the 0.5 – 0.8 m scale. At the 3D Laser Scanning scale of observation, the roughness of the sampled surfaces has a very complex behaviour. Roughness of surface is determined at different scales by different morphologic features as also outlined in (Shepard *et al*., 2001). The Hurst exponent (*H*) is the most useful parameter to identify the break points (fig. 4c and table I). The surface roughness transitions for tephra are controlled by the grain size of deposits. This is clearly demonstrated by the morphologic features of S8 and S11 samples. Coarse tephra (S8) has medium to low *H* values, and the average size of grain forming the surface controls the surface roughness (figs. 4a and c). The roughness of fine tephra (S11), on the other hand, is essentially controlled by wavy pattern of background at large scale (figs. 4a and c).

Surface roughness parameters (σ, λ and *H*) show a strong correlation with the size of the grain size of the tephra deposits (especially σ and *H*) and with the tephra thickness in terms of percentage of bedrock exposed on the analysed sample (especially σ and λ). These preliminary results thus indicate that, at least at the metre scale of observation, the roughness of pyroclastic deposit surfaces could be used as a mapping tool for mapping pyroclastic deposits in volcanoes. Further analysis on tephra at scale of observation in the range 1 -10 m necessitate to completely define the surface roughness of these volcanic surface to cover the scales of observations of high-resolution remote sensing platforms.

Finally, the 3D Laser Scanning method allows the acquisition of high resolution (up to 0.1 mm along the z axis) digital elevation models of natural surfaces, permitting to perform accurate 1D (profiles) and 2D (surface) morphologic analysis. The change in grain size distribution for unconsolidated pyroclastic deposits affects the relative surface roughness producing thus different surface textures.

Acknowledgments

The research was supported by funds from the MIUR Project «Sviluppo Nuove Tecnologie per la Protezione e Difesa del Territorio dai Rischi Naturali» and from the Italian Dipartimento Protezione Civile at the Istituto Nazionale di Geofisica e Vulcanologia (supervisor: M.T. Pareschi).

REFERENCES

Akiyama, H and S. Sasaki (2002): Effects of rock coating on reflectance spectra of rock samples. Solar System. *Remote Sensing Symposium, Pittsburgh, Pennsylvania*, September 20-21.

Allard, P., B. Behncke, S. D'Amico, M. Neri and S. Gambino (2006): Mount Etna 1993-2005: Anatomy of an Evolving Eruptive Cycle, *Earth-Science Rev.*, **78**, 85-114.

Amelung, F., S. Jonsson, H. Zebker and P. Segall (2000): Widespread uplift and «trapdoor» faulting on Galápagos volcanoes observed with radar interferometry, *Nature*, **407**, 993-996.

Andronico, D., S. Branca, S. Calvari, M. Burton, T. Caltabiano, R. A. Corsaro, P. Del Carlo, G. Garfi, L. Lodato, L. Miraglia, F. Muré, M. Neri, E. Pecora, M. Pompilio, G. Salerno and L. Spampinato (2005): A multi-disciplinary study of the 2002-03 Etna eruption: insights into a complex plumbing system, *Bulletin of Volcanology*, **67**, 314-330.

Anzidei, M., A. Esposito and F. De Giosa (2006): The dark side of the Albano crater lake, *Annals of Geophysics*, **49**, 1275-1287.

Anzidei, M., M.L. Carapezza, A. Esposito, G. Giordano, M. Lelli and L. Tarchini (2008): The Albano maar lake high resolution bathymetry and dissolved CO_2 budget (Colli Albani volcano, Italy): Constraints to hazard evaluation, *Jour. Volcanol. Geotherm. Res*., **171**, 258-268.

Behncke, B. and M. Neri (2003a): The July-August 2001 eruption of Mt. Etna (Sicily), *Bulletin of Volcanology*, **65**, 461-476.

Behncke, B. and M. Neri (2003b): Cycles and trends in the recent eruptive behaviour of Mount Etna (Italy), *Canadian Journal of Earth Sciences*, **40**, 1405-1411.

Behncke, B., M. Neri and A. Nagay (2005): Lava flow hazard at Mount Etna (Italy): New data from a GIS-based study, in «Kinematics and dynamics of lava

flows» (M. MANGA and G. VENTURA, eds.), *Spec. Pap. Geol. Soc. Am.*, **396-13**, 187-205.

BRANCA, S. and P. DEL CARLO (2004): Eruptions of Mt. Etna during the past 3200 years: A revised compilation integrating the historical and stratigraphic records, in «Mt. Etna: Volcano Laboratory» (A. BONACCORSO, S. CALVARI, M. COLTELLI, C. DEL NEGRO and S. FALSAPERLA, eds.), *Geophysical Monograph Series*, **143**, 1-27.

BRIOLE, P., D. MASSONNET and C. DELACOURT (1997): Post eruptive deformation associated with the 1986-1987 and 1989 lava flows of Etna detected by radar interferometry, *Geophys. Res. Lett.*, **24**, 37-40.

BULMER, M.H., B.A. CAMPBELL and J. BYRNES (2001): Field studies and radar remote sensing of silicic lava flows, in *Proc. Lunar and Planetary Science Conference XXXII,* Abstract # 1850.

BUTLER, J.B., S.N. LANE and J.H. CHANDLER (1998): Assessment of DEM quality for characterizing surface roughness using close range digital photogrammetry, *Photogrammetric Record*, **16**, 271-291.

CALVARI, S., M. NERI and H. PINKERTON (2002): Effusion rate estimations during the 1999 summit eruption on Mount Etna, and growth of two distinct lava flow fields, *Jour. Volcanol. Geotherm. Res.*, **119**, 107-123.

CAMPBELL B.A. and M.K. SHEPARD (1996): Lava flow surface roughness and depolarized radar scattering, *J. Geophys. Res.*, **101**, 18941-18951.

CASACCHIA, R., F. MAZZARINI, C. SPINETTI, L. COLINI, M. NERI, B. BEHNCKE, M. F. BUONGIORNO, V. DESANTIS, A. GRIGNETTI and R. SALVATORI (2006): Riflettanza di superfici vulcaniche: la campagna 2003 sul Monte Etna, *Rivista Italiana di TELERILEVAMENTO*, **36**, 55-67.

FAVALLI, M., F. MAZZARINI, M. T. PARESCHI and E. BOSCHI (2004): Role of local wind circulation in plume monitoring at Mt. Etna volcano (Sicily): Insights from a mesoscale numerical model, *Geophys. Res. Lett.*, **31**, L09105, doi: 10.1029/2003GL019281.

FROGER, J. L., O. MERLE and P. BRIOLE (2001): Active spreading and regional extension at Mount Etna imaged by SAR interferometry, *Earth Planet. Sci. Lett.*, **187**, 245-258.

JANZA, F.J., H.M BLUE and J.E. JOHNSTON eds. (1975): Manual of Remote Sensing, vol. I, Theory, Instruments and Techniques, *American Society of Photogrammetry*, 1-867.

MAZZARINI, F., M. T. PARESCHI, M. FAVALLI, I. ISOLA, S. TARQUINI and E. BOSCHI (2005): Morphology of basaltic lava channels during the Mt. Etna September eruption from airborne laser altimeter data, *Geophys. Res. Lett.*, **32**, L04305, doi:10.1029/2004GL021815.

MAZZARINI, F., M. PARESCHI, M. FAVALLI, I. ISOLA, S. TARQUINI and E. BOSCHI (2007): Lava flow identification and aging by means of Lidar intensity: Mount Etna case, *J. Geophys. Res.*, **112**, B02201, doi: 10.1029/2005JB004166.

MORGAN, L.A., W.C. SHANKS II, D.A. LOVALVO, S.Y. JOHNSON, W.J. STEPHENSON, K.L. PIERCE, S.S. HARLAN, C.A. FINN, G. LEE, M. WEBRING, B. SCHULZE, J. DUHN, R. SWEENEY and L. BALISTRIERI (2003): Exploration and discovery in Yellowstone Lake: results from high-resolution sonar imaging, seismic reflection profiling, and submersible studies, *Jour. Volcanol. Geotherm. Res.*, **122**, 221-242.

MORRIS, A.R., F.S. ANDERSON, P.J. MOUGINIS-MARK, A.F.C. HALDEMANN and T.K.P. GREGG (2006): Initial analysis of topographic roughness of Martian and Hawaiian terrains, in *Proc. Lunar and Planetary Science Conference XXXVII*, Abstract # 2064.

OROSEI R., R. BIANCHI, A. CORADINI, S. ESPINASSE, C. FEDERICO, A. FERRICCIONI and I. GAVRISHIN (2003): Self-affine behaviour of Martian topography at kilometer scale from Mars Orbiter Laser Altimeter data, *J. Geophys. Res.*, **108**, 8023, doi:10.1029/2002JE001883.

PESCI, A., M. FABRIS, D. CONFORTI, F. LODDO, P. BALDI and M. ANZIDEI (2007): Integration of ground-based laser scanner and aerial digital photogrammetry for topographic modelling of Vesuvio volcano, *Jour. Volcanol. Geotherm. Res.*, **162**, 123-138.

SGAVETTI, M., L. POMPILIO and S. MELI (2006): Reflectance spectroscopy (0.3 – 2.5 μm) at various scales for bulk-rock identification, *Geosphere*, **2**, 142-160.

SHEPARD, M.K., R.A. BRACKETT and R.E. ARVIDSON (1995): Self-affine (fractal) topography: Surface parameterization and radar scattering, *J. Geophys. Res.*, **100**, 11709-11718.

SHEPARD, M.K. and B.A. CAMPBELL (1999): Radar scattering from a self-affine fractal surface: near-nadir regime, *Icarus*, **141**, 156-171.

SHEPARD, M.K., B.A CAMPBELL, M.H. BULMER, T.G. FARR, L.R. GADDIS J. and J. PLAUT (2001): The roughness of natural terrain: A planetary and remote sensing perspective, *J. Geophys. Res.*, **106**, 32777-32795.

STEVENS, N.F., G. WADGE, C.A. WILLIAMS, J.G. MORELY, J.-P. MULLER, J.B. MURRAY and M. UPTON (2001): Surface movements of emplaced lava flows measured by synthetic aperture radar interferometry, *J. Geophys. Res.*, **106**, 11293-11313.

TADDEUCCI, J., M. POMPILIO and P. SCARLATO (2002): Monitoring the explosivity of the July-August 2001 eruption of Mt. Etna Italy by ash characterization, *Geophys. Res. Lett.*, **29**, doi:10.10.29/2001GL014372.

TURCOTTE, D.L. (1997): *Fractals and chaos in Geology and Geophysics*, 2nd ed., (Cambridge Univ. Press, New York), pp. 1-398.

(received March 5, 2008;
accepted June 23, 2008)